

# Vortices in nonequilibrium photon condensates

Vladimir Gladilin and Michiel Wouters

*TQC, Universiteit Antwerpen, Universiteitsplein 1, B-2610 Antwerpen, Belgium*

(Dated: June 22, 2020)

We present a theoretical study of vortices in arrays of photon condensates. Even when interactions are negligible, as is the case in current experiments, pumping and losses can lead to a finite vortex core size. While some properties of photon condensate vortices, such as their self-acceleration and the generation of vortex pairs by a moving vortex, resemble those in interacting polariton condensates far from equilibrium, in several aspects they differ from previously studied systems: the vortex core size is determined by the balance between pumping and tunneling, the core appears oblate in the direction of its motion and new vortex pairs can spontaneously nucleate in the core region.

*Introduction* – The experimental study of planar optical systems has spurred the interest in studying the properties of light from the point of view of quantum fluids [1]. Superfluidity [2] and quantized vortices [3] as one of its hallmarks [4] have developed into a rich research domain with recent studies addressing the Berezinskii-Kosterlitz-Thouless phase transition [5–7], the Kibble-Zurek mechanism [8–10] and Kardar-Parisi-Zhang dynamics of the superfluid phase [11–15]. Moreover, planar optical systems have been identified as promising platforms to perform analog computation, with potential applications in NP hard optimization problems. These ideas have been implemented in exciton-polariton condensates [16–18], parametric oscillators [19, 20], coupled laser arrays [21] and a proposal was done for coupled Bose-Einstein condensates (BECs) of photons in a dye filled cavity [22].

This latter photon condensate system [23–26] is in good approximation an ideal Bose gas, which at first sight limits its possibilities for the study of superfluidity. The ideal Bose gas has a zero Landau critical velocity and has no well-defined quantized vortices because the core size becomes as large as the entire system [4]. This is related to the infinite compressibility of the ideal Bose gas, which leads through the fluctuation-dissipation relation to large density fluctuations [27] that prevent the emergence of a well defined phase degree of freedom. However, because of cavity mirror losses, which are compensated by external pumping, photon condensates do differ from the ideal Bose gas. Thanks to the interplay between pumping and dissipation, density fluctuations can be reduced so that the photon phase becomes well defined [28].

Experimentally, it has become possible to create arrays of photon condensates by controllably coupling them through tunneling [22, 29]. In such systems a well defined phase can be combined with spatial variations, which opens up the possibility to study quantized vortices. Previous studies of vortices [30, 31] and the BKT transition in nonequilibrium polariton condensates [6, 7] have shown that deviations from nonequilibrium strongly affect the properties of single vortices as well as their interactions and annihilation rates. In these works, an intrinsic nonlinearity was included, such that the driving and dissipation formed a correction to the equilibrium vortex structure. In photon BECs, in contrast, driving and dissipation dominate the vortex structure and the deviation

from equilibrium becomes essential in order to obtain a finite vortex core size.

*Model* – One of the advantages of photon condensates is that their microscopic physics is well understood. The thermalization of the photons through repeated emission and absorptions by the dye molecules is achieved thanks to the Kennard-Stepanov relation [32–34] that sets a correspondence between the emission ( $B_{21}$ ) and absorption ( $B_{12}$ ) coefficients:  $B_{12} = e^{\beta\Delta} B_{21}$ , where  $\Delta$  is the detuning between the cavity and the dye transition frequencies and  $\beta = 1/(k_B T)$  is the inverse temperature. For a single mode system, rate equations give a good description of the photon density dynamics [35, 36]. For the extension to coupled cavities, the simplest model is given by a generalized Gross-Pitaevskii equation (gGPE) for the photon amplitudes [28]:

$$i\hbar \frac{\partial \psi(\mathbf{x})}{\partial t} = -(1 - i\kappa)J \sum_{\mathbf{x}' \in \mathcal{N}_{\mathbf{x}}} \psi(\mathbf{x}') + V(\mathbf{x})\psi(\mathbf{x}) + \frac{i}{2} [B_{21}M_2(\mathbf{x}) - B_{12}M_1(\mathbf{x}) - \gamma]\psi(\mathbf{x}). \quad (1)$$

It describes photons with loss rate  $\gamma$  subject to an external potential  $V$  that hop to the nearest neighbor cavities, labeled by  $\mathbf{x}'$ , at tunneling rate  $J$ . The photons are coupled to the dye molecules whose ground (excited) state occupation is denoted by  $M_{1(2)}$  satisfying at all times  $M_1(\mathbf{j}) + M_2(\mathbf{j}) = M$ , where  $M$  is the number of dye molecules at each lattice site. The Kennard-Stepanov relation gives rise to energy relaxation with dimensionless strength

$$\kappa = \frac{1}{2}\beta B_{12}M_1. \quad (2)$$

Our model does not include photonic interaction, which is quite negligible in recent experiments [37], except for a slow thermo-optical nonlinearity [38], which does not affect the physics over the time scales relevant for this study.

Equation (1) is deterministic and it fails to describe the fluctuations of the photon gas. These are included by adding a unit complex number with random phase to the field amplitude at the rate of the spontaneous photon emissions [36, 39].

The evolution of the number of excited molecules due to interactions with the photons is opposite to the change in number of photons due to emission (both deterministic and stochastic), absorption and energy relaxation. In order to compensate for the loss of energy in the system, external excitation with a pumping laser is needed to balance the photon losses:  $P_{\text{pump}} = \gamma \bar{n}$ , where  $\bar{n}$  is the targeted mean photon number.

For a single photonic mode, two different regimes can be identified [40, 41] in the parameter space of mean photon number  $\bar{n}$  and effective molecular reservoir size  $M_{\text{eff}} = (M + \gamma e^{-\beta\Delta}/B_{21})/[2 + 2 \cosh(\beta\Delta)]$ : (i) a large fluctuation ‘grandcanonical’ regime for small photon number  $\bar{n}^2 \ll M_{\text{eff}}$ , where  $\langle (n - \bar{n})^2 \rangle \approx \bar{n}^2$  and (ii) a small fluctuation ‘canonical’ regime for  $\bar{n}^2 \gg M_{\text{eff}}$ , where  $\langle (n - \bar{n})^2 \rangle \approx M_{\text{eff}} \ll \bar{n}^2$ . Only in the latter case, a well defined phase of the condensate emerges. In the other case, frequent fluctuations to zero density lead to reinitialization of the condensate with an arbitrary phase. In this regime, the phase is not a slow degree of freedom with its own effective dynamics as in the case of superfluids. This is consistent with the thermal equilibrium nature of the ideal Bose gas, which does not show real superfluid behavior.

In the canonical regime, when two or more photon modes are coupled by tunnelling, the density fluctuations are determined by a competition between tunnelling and pumping/losses [28]. In the absence of losses, the particle exchange causes density fluctuations to go to the large grandcanonical value. The addition of pumping and losses instead tends to fix the instantaneous local density to the targeted one and suppresses density fluctuations. The phase can then still be a good long wavelength degree of freedom. It is only in this parameter regime that well defined vortices can be studied.

*Results* – Numerical simulations were performed on a relatively large lattice of  $101 \times 101$  coupled photon condensates. An external potential of magnitude  $V = -J$  at the border of the lattice, and  $V = -2J$  in the corners is applied in order to make the condensate density homogeneous. In the absence of this potential offset, the condensate density profile becomes highly inhomogeneous, which encumbers the analysis.

Two examples of vortices in an array of photon condensates are shown in Fig. 1. The simulations were started with a phase winding of  $2\pi$  and then evolved until the density and phase patterns around the vortex core were stabilized. In both simulations, it is seen from the spiral form of phase pattern that in addition to the azimuthal flow, there is a radial flow out of the vortex core. This phenomenon is well known from studies of the complex Ginzburg-Landau equation [42] and theory of vortices in nonequilibrium polariton condensates [30, 31]. The physical origin of the outward currents is the photon density suppression at the vortex core, leading to less radiative losses while pumping remains the same. The resulting excess energy is carried away by the radial photon currents.

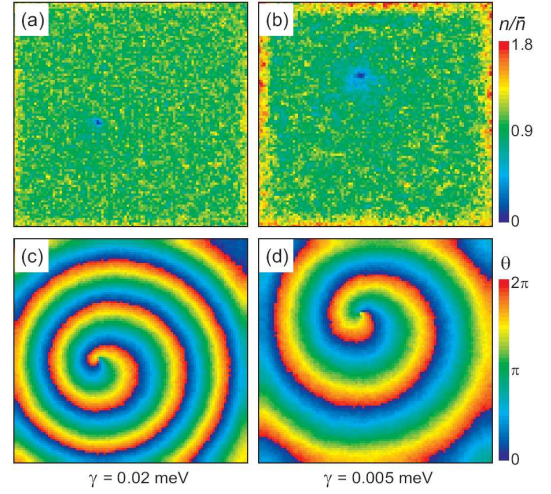


FIG. 1. Snapshots of the photon density  $n$  [panels (a) and (b)] and the phase of the order parameter  $\theta$  [panels (c) and (d)] for  $B_{21} = 10^{-6}$  meV ( $\kappa = 0.763$ ),  $J = 0.02$  meV and two different values of the loss rate:  $\gamma = 0.02$  meV [panels (a) and (c)] and  $\gamma = 0.005$  meV [panels (b) and (d)]. The other parameters of the simulation are  $k_B T = 25$  meV,  $\Delta/(k_B T) = -7.2$ ,  $M = 5 \times 10^{10}$ ,  $\bar{n} = 5 \times 10^4$ .

In the usual case of interacting bosons at thermal equilibrium, the vortex core size is determined by the interaction energy, which sets the healing length. This length scale tends to infinity in the limit of vanishing interactions. This limit is recovered in the present simulations when losses go to zero. However, driving and dissipation provide an alternative mechanism to restrict the vortex core size: within their finite life time, the photons can only travel over a limited distance. This reasoning suggests an inverse proportionality between the vortex core radius and the loss rate. Analytical considerations based on the linearized equations for density and phase fluctuations [28] lead to the estimate for the vortex core radius  $r_v \propto \sqrt{J/\gamma}$ .

The increase of the vortex core radius with increasing  $J/\gamma$  is confirmed by the numerical simulations in Fig. 1 [compare panel (a) with larger losses than in panel (b)]. Since the radial currents serve to carry away the excess excitation from the vortex core region, they decrease with decreasing pumping and losses. This is seen from the larger distance between the spiral arms in panel (d) as compared to panel (c). The reduction of stimulated relaxation of dye molecules in the vortex core region leads to a local increase of the number of excited molecules (see supplementary information, Fig. s1). In line with the increased core region for smaller losses, the size of this molecular ‘hot spot’ increases with decreasing losses.

So far, we have only discussed the density and phase profiles of the vortex, but also the motion of the vortex core itself appears to be interesting, as is illustrated in Fig. 2 (a) and (b). In contrast to an equilibrium quantum fluid, where vortices move along with the condensate, the vortex core now shows self-acceleration. This

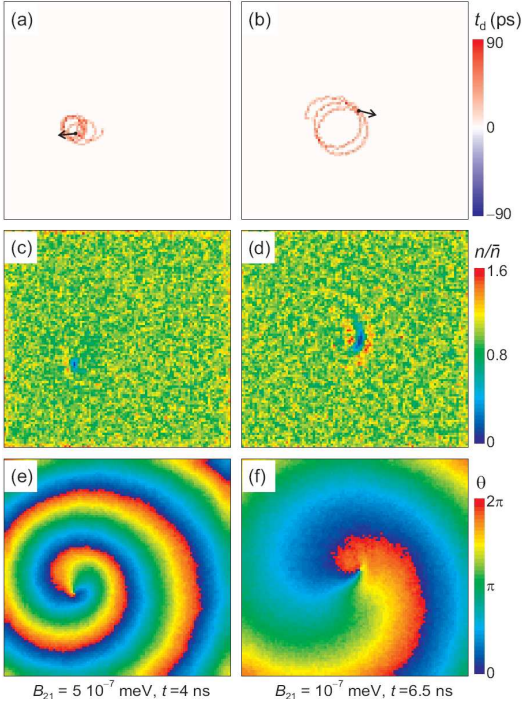


FIG. 2. (a-b) Vortex trajectories: the color codes the time the core dwells in a given pixel with the sign of the dwelling time representing the vorticity sign. The arrow indicates the velocity at the final time of the simulation. Panels (c-d) show the photon density profile at this instant, panels (e-f) the phase profile. Parameters are the same as in Figs. 1(a) and (c), except for  $B_{21}$ .

phenomenon has been described previously in the context of the cGLE [42] and in a related phenomenological model for polariton condensates [30, 31]. The present simulations show that the acceleration of the vortex core also appears in the absence of interparticle interactions.

The vortex follows to a good approximation a circular trajectory. Deviations are caused by the fluctuations due to spontaneous emission and by interactions with the sample boundaries. The curvature of the trajectory can be understood from the Magnus effect [43, 44] that is a consequence of a nonzero vortex core velocity  $v_{vc}$  with respect to the surrounding condensate (due to self-acceleration). Comparing panels (a) and (b) of Fig. 2, it is clear that the curvature of the trajectory decreases with decreasing emission coefficient  $B_{21}$ . This coefficient not only affects the conversion between photons and excited molecules, but also the energy relaxation parameter  $\kappa$ , cf. Eq. (2). We have verified in other simulations (see supplementary information, Figs. s2 and s3) by independently varying  $B_{21}$  and  $\kappa$  (could be physically implemented by changing the temperature) that the increase in the curvature of the trajectory is mainly due to the increase of  $B_{21}$  and not of  $\kappa$ . Some intuition for this dependence can be obtained by considering the ratio  $J/B_{21}$ , which expresses the tunneling strength in the energy scale of the interaction between photons

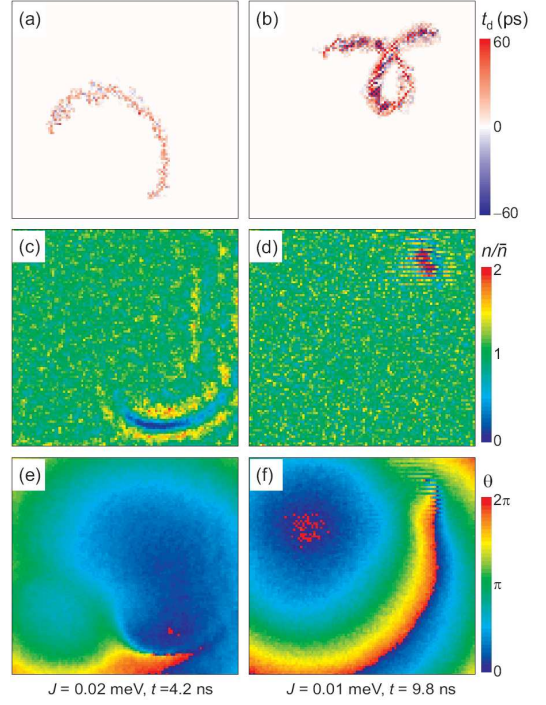


FIG. 3. Formation of baby vortices inside the core when the tunneling rate  $J$  is reduced. The panels give the same information as in Fig. 2. Parameters are the same as in Fig. 1 (a) and (c), except for a reduced value of  $J$  for panels (b), (d) and (f) and a significantly smaller  $B_{21} = 2.5 \times 10^{-8}$  meV for all panels.

and molecules. Increasing  $J/B_{21}$  can be thought of as an increase in resolution within the continuum limit of the lattice model. This change is then accompanied by a magnification of the vortex trajectory picture. When, on the other hand,  $\kappa$  is varied independently, the curvature of the vortex trajectory appears to remain nearly unaltered.

Apart from the change in trajectory curvature, reducing  $B_{12}$  leads to an increase in size and a deformation of the core. In panel (d) the core is significantly elongated in the direction approximately perpendicular to the direction of the vortex motion, that is indicated by the arrow in panel (b) (see also Fig. s4 in Supplementary information). This contrasts with vortices in superconductors, where due to a long healing time of the order parameter the core of a fast moving vortex elongates in the direction of its motion [45, 46]. Apart from the core deformation, also photon density maxima behind and in front of the core appear. In these high density regions, the photon losses are higher, such that the radial currents emitted by the vortex core are partially drained here. This is reflected in the phase profile [compare panel (f) to panel (e)] as a slower winding of the spiral arms.

More exotic physics appears when the emission coefficient  $B_{21}$  and, correspondingly, the energy relaxation parameter  $\kappa$  are further reduced. The vortex core then turns out to be unstable as most clearly illustrated in the



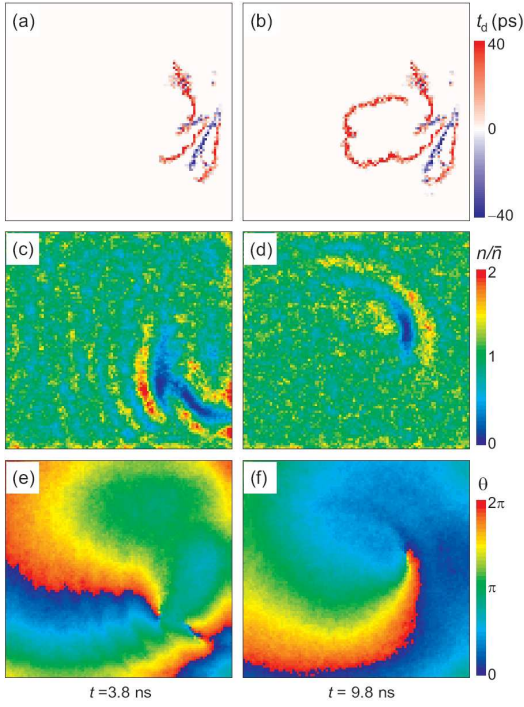


FIG. 4. Trajectories of vortices (red) and antivortices (blue) up to 3.8 ns (a) and 9.8 ns (b), when the original vortex approaches the boundary. Formation of new pairs at the boundary and their recombination can be seen. The density and phase after 3.8 ns are shown in panels (c,e), where in addition to the original vortex, a clear vortex-antivortex pair is visible. Panels (d,f) show density and phase after 9.8 ns, when only a single vortex survives after it has moved away from the edge of the cavity array. Parameters are the same as in Fig. 1(b) and (d), except for  $B_{21} = 2.5 \times 10^{-8}$  meV.

right hand side panels (b,d,f) of Fig. 3. In panels (a,b) an area with both negative and positive vorticity can be recognized, while the imprinted vorticity is positive, which is reflected in the long distance behavior of the phase. At short distances on the other hand, one sees the formation of baby vortex-antivortex pairs. Correspondingly in the density profile, see panel (d), the vortex core is no longer a simple minimum of the density, but it shows large density variations. Because the vortex core is now filled, the radial currents become much weaker, such that the spiral form of the vortex almost disappears.

The reason for the formation of baby vortices is that the low density in the vortex core enhances the phase fluctuations caused by spontaneous emission. Loosely speaking, one could compare these baby vortices with the spontaneous formation of vortices in the Berezinskii-Kosterlitz-Thouless (BKT) phase transition, which occurs when the density drops below a (temperature dependent) critical value [4].

In Fig. 4, we show a situation where a vortex approaches the boundary of the sample. The appearance of blue pixels in panels (a) and (b) demonstrates that new vortex-antivortex pairs are generated. Density and phase

profiles at the time when the vortex is close to the boundary are shown in panels (c,e). A new vortex-antivortex pair is clearly visible. Panel (b) shows that the original vortex actually recombines with one of the newly created antivortices and that the other member of the pair continues as the only remaining vortex when it moves away from the boundary, see panels (d,e). The production of vortex-antivortex pairs at the boundary resembles the creation of baby vortices inside the vortex core, but it already happens at larger ratio  $J/\gamma$  (where the vortex core is more stable), with the boundary facilitating the formation of new pairs.

The generation of vortex-antivortex pairs by fast moving vortices was already seen in simulations for polariton condensates [31, 47], where we used a continuum model that was discretized only for the numerical solution of the partial differential equation. In contrast, for photon condensates, it is crucial to use a discrete set of coupled cavities in order to keep the density fluctuations in check and to limit the vortex core size.

*Conclusions and outlook* – Our study of arrays of coupled photon condensates has shown that the formation of quantized vortices with a well defined core is possible in the canonical regime if the tunneling strength is small enough with respect to the loss rate. Because the vortex properties are entirely determined by the interplay between tunneling and pumping, they feature unusual properties when compared to vortices in traditional superfluids.

We have recovered several features that were previously obtained for nonequilibrium polariton condensates, such as radially diverging particle flows from the vortex core [42], self-accelerated vortex motion [30] and the production of vortex-antivortex pairs in interactions with the sample boundary [31]. Novel features are the vortex core instability with the formation of “baby” vortices and the elongation of the core that is quasi-perpendicular to its velocity.

In analogy with polariton condensates [30, 31], it is expected that the radial flows will lead to vortex-antivortex repulsion and inhibit vortex-antivortex recombination. A preliminary case study (see supplementary material Fig. s5) confirms this expectation, but a comprehensive analysis of the interactions between vortices is beyond the scope of the present work.

Our results pave the way for studies of photon condensates with multiple vortices, which may be generated by phase imprinting, in quenches through the Kibble-Zurek mechanism or thermally activated as in the BKT transition. Finally, vortices may also play a role in the formation of metastable states in proposed schemes for analog solving of optimization problems [22].

Our theoretical predictions rely upon a semiclassical model which is based on microscopic physics that is well understood and should be accessible to experiments where photon condensates can be coupled in a controlled manner [22, 29].

*Acknowledgements* – We are grateful to Jan Klaers,

Fahri Ozturk, Martin Weitz and Wouter Verstraelen for

stimulating discussions. VG was financially supported by the grant UA-BOF-FFB150168.

- 
- [1] I. Carusotto and C. Ciuti, *Reviews of Modern Physics* **85**, 299 (2013).
  - [2] A. Amo, J. Lefrère, S. Pigeon, C. Adrados, C. Ciuti, I. Carusotto, R. Houdré, E. Giacobino and A. Bramati, *Nat. Phys.* **5**, 805 (2009).
  - [3] K. G. Lagoudakis, M. Wouters, M. Richard, A. Baas, I. Carusotto, R. André, Le Si Dang and B. Deveaud-Plédran, *Nat. Phys.* **4**, 706 (2008).
  - [4] L. P. Pitaevski and S. Stringari, *Bose-Einstein condensation* (Oxford University Press, 2016).
  - [5] D. Caputo, D. Ballarini, G. Dagvadorj, C. S. Muñoz, M. De Giorgi, L. Dominici, K. West, L. N. Pfeiffer, G. Gigli, F. P. Laussy, M. H. Szymańska and D. Sanvitto, *Nat. Mat.* **17**, 145 (2018).
  - [6] G. Wachtel, L. M. Sieberer, S. Diehl and E. Altman, *Phys. Rev. B* **94**, 104520 (2016).
  - [7] L. M. Sieberer, G. Wachtel, E. Altman and S. Diehl, *Phys. Rev. B* **94**, 104521 (2016).
  - [8] P. Comaron, G. Dagvadorj, A. Zamora, I. Carusotto, N. P. Proukakis, and M. H. Szymańska, *Dynamical critical exponents in driven-dissipative quantum systems*, *Phys. Rev. Lett.* **121**, 095302 (2018).
  - [9] M. Kulczykowski and M. Matuszewski, *Phys. Rev. B* **95**, 075306 (2017).
  - [10] M. Wouters and W. Verstraelen, *Phys. Rev. A* **101**, 043826 (2020).
  - [11] D. Squizzato, L. Canet and A. Minguzzi, *Phys. Rev. B* **97**, 195453 (2018).
  - [12] V. N. Gladilin, K. Ji, and M. Wouters, *Phys. Rev. A* **90**, 023615 (2014).
  - [13] L. He, L. M. Sieberer, E. Altman, and S. Diehl, *Phys. Rev. B* **92**, 155307 (2015).
  - [14] E. Altman, L. M. Sieberer, L. Chen, S. Diehl, and J. Toner, *Phys. Rev. X* **5**, 011017 (2015).
  - [15] L. M. Sieberer, M. Buchhold, and S. Diehl, *Reports on Progress in Physics* **79**, 096001 (2016).
  - [16] N. G. Berloff, M. Silva, K. Kalinin, A. Askitopoulos, J. D. Töpfer, P. Cilibrizzi, W. Langbein and P. G. Lagoudakis, *Nat. Mater.* **16**, 1120 (2017).
  - [17] P. Lagoudakis and N. G. Berloff, *New J. Phys.* **19**, 125008 (2017).
  - [18] K. Kalinin, P. G. Lagoudakis, N. G. Berloff, *Phys. Rev. B* **97**, 094512 (2018).
  - [19] P. L. McMahon, A. Marandi, Y. Haribara, R. H. C. Langrock, S. Tamate, T. Inagaki, H. Takesue, S. Utsunomiya, K. Aihara, R. L. Byer, M. M. Fejer and H. Mabuchi, Y. Yamamoto, *Science* **354**, 614 (2016).
  - [20] Y. Yamamoto, K. Aihara, T. Leleu, K. Kawarabayashi, S. Kako, M. Fejer, K. Inoue and H. Takesue *NPJ Quant. Inf.* **3**, 49 (2017).
  - [21] C. Tradonsky, I. Gershenzon, V. Pal, R. Chriki, A. A. Friesem, O. Raz and N. Davidson *Science Advances* **5**, 4530 (2019).
  - [22] B. Kassenberg, M. Vretenar, S. Bissesar, J. Klaers, *arXiv:2001.09828*.
  - [23] J. Klaers, J. Schmitt, F. Vewinger, and M. Weitz, *Nature* **468**, 545 (2010).
  - [24] J. Marelic, L. F. Zajiczek, H. J. Hesten, K. H. Leung, E. Y. X. Ong, F. Mintert and R. A. Nyman, *N. J. Phys.* **18**, 103012 (2016).
  - [25] B. T. Walker, L. C. Flatten, H. J. Hesten, F. Mintert, D. Hunger, A. A. P. Trichet, J. M. Smith and R. A. Nyman, *Nat. Phys.* **14**, 1173 (2018).
  - [26] S. Greveling, K. L. Perrier and D. van Oosten, *Phys. Rev. A* **98**, 013810 (2018).
  - [27] M. Klawunn, A. Recati, L. P. Pitaevskii and S. Stringari, *Phys. Rev. A* **84**, 033612 (2011).
  - [28] V. N. Gladilin and M. Wouters, *Phys. Rev. A* **101**, 043814 (2020).
  - [29] D. Dung, C. Kurtscheid, T. Damm, J. Schmitt, F. Vewinger, M. Weitz and J. Klaers, *Nat. Phot.* **11**, 565 (2017).
  - [30] V. N. Gladilin and M. Wouters, *New J. Phys.* **19**, 105005 (2017).
  - [31] V. N. Gladilin and M. Wouters, *J. Phys. A* **52**, 1751 (2019).
  - [32] E. H. Kennard, *Phys. Rev.* **11**, 29 (1918).
  - [33] B. I. Stepanov, *Dokl. Akad. Nauk SSSR* **112**, 839 (1957). [*Sov. Phys. Dokl.* **2**, 81 (1957)].
  - [34] P. Moroshkin, L. Weller, A. Saß, J. Klaers and M. Weitz, *Phys. Rev. Lett.* **113**, 063002 (2014).
  - [35] J. Schmitt, *Journal of Physics B*, **51**, 173001 (2018).
  - [36] W. Verstraelen and M. Wouters, *Phys. Rev. A* **100**, 013804 (2019).
  - [37] M. Radonji, W. Kopylov, A. Bala, and A. Pelster, *N. J. Phys.* **20**, 055014 (2018).
  - [38] H. Alaeian, M. Schedensack, C. Bartels, D. Peterseim and M. Weitz, *N. J. Phys.* **19**, 115009 (2017).
  - [39] C. Henry, *IEEE Journal of Quantum Electronics* **18**, 259 (1982).
  - [40] J. Klaers, J. Schmitt, T. Damm, F. Vewinger, and M. Weitz, *Phys. Rev. Lett.* **108**, 160403 (2012).
  - [41] J. Schmitt, T. Damm, D. Dung, F. Vewinger, J. Klaers and M. Weitz, *Phys. Rev. Lett.* **112**, 030401 (2014).
  - [42] I. S. Aranson and L. Kramer, *Rev. Mod. Phys.* **74**, 99 (2002).
  - [43] H. E. Hall and W. F. Vinen, *Proc. Roy. Soc. A* **238**, 204 (1956).
  - [44] E. B. Sonin *Phys. Rev. B* **55**, 485 (1997).
  - [45] D. Y. Vodolazov and F. M. Peeters, *Phys. Rev. B* **76**, 014521 (2007).
  - [46] J. Van de Vondel, V. N. Gladilin, A. V. Silhanek, W. Gillijns, J. Tempere, J. T. Devreese, and V. V. Moshchalkov, *Phys. Rev. Lett.* **106**, 137003 (2011).
  - [47] V. N. Gladilin and M. Wouters, *Phys. Rev. B* **100**, 214506 (2019).

## SUPPLEMENTARY FIGURES

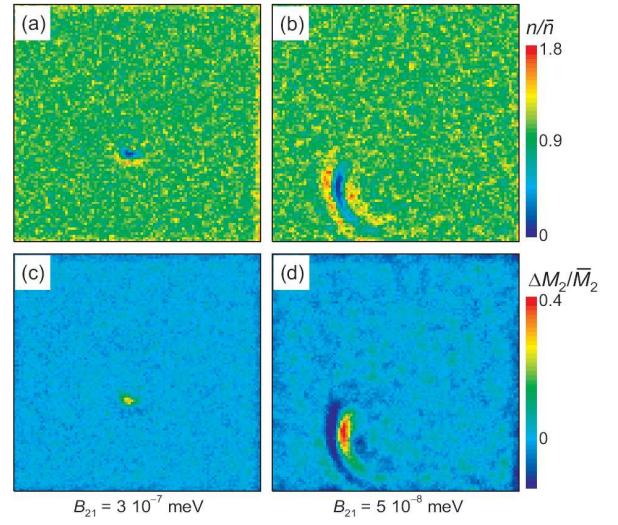


FIG. s1. Snapshots of the photon density  $n$  [panels (a) and (b)] and the distribution of deviations of the number of excited molecules from its average value  $\Delta M_2 \equiv M_2 - \bar{M}_2$  [panels (c) and (d)] for  $k_B T = 25$  meV,  $\Delta/(k_B T) = -7.2$ ,  $M = 5 \times 10^{10}$ ,  $\bar{n} = 5 \times 10^4$ ,  $J = 0.02$  meV,  $\gamma = 0.02$  meV and two different values of the emission coefficient:  $B_{21} = 3 \times 10^{-7}$  meV ( $\kappa = 0.229$ ), [panels (a) and (c)] and  $B_{21} = 5 \times 10^{-8}$  meV ( $\kappa = 0.038$ ) [panels (b) and (d)]. There is a clear anticorrelation between the distributions of  $n$ , on the one hand, and  $M_2$ , on the other hand.

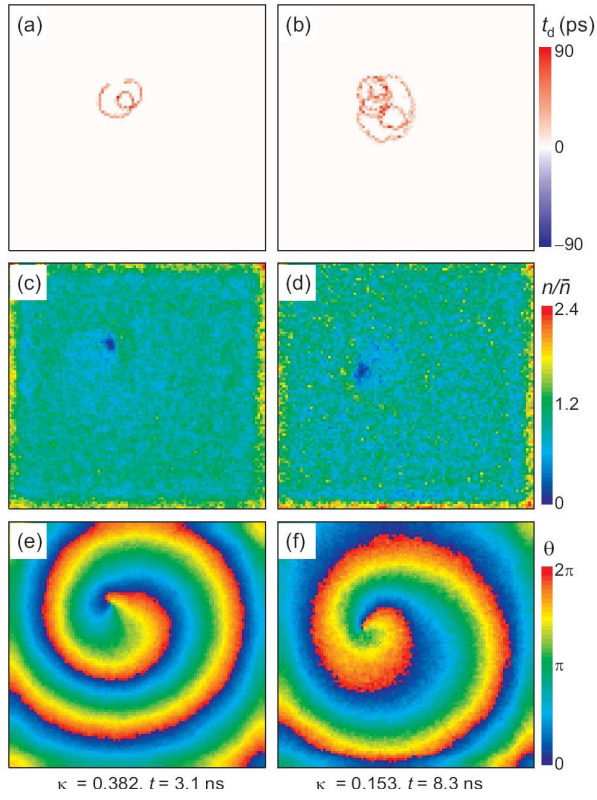


FIG. s2. Vortex trajectories within the time interval  $(0, t)$  [panels (a) and (b)] and snapshots of the photon density  $n$  [panels (c) and (d)] and the phase of the order parameter  $\theta$  [panels (e) and (f)] at the time moment  $t$  for  $\Delta/(k_B T) = -7.2$ ,  $M = 5 \times 10^{10}$ ,  $\bar{n} = 5 \times 10^4$ ,  $J = 0.02$  meV,  $\gamma = 0.005$  meV,  $B_{21} = 5 \times 10^{-7}$  meV and two different values of  $\kappa$ , which is considered here as an independent parameter:  $\kappa = 0.382$  [panels (a), (c) and (e)] and  $\kappa = 0.153$  [panels (b), (d) and (f)]. A decrease of  $\kappa$  results in an increase the of density and phase fluctuations, induced by the Josephson junctions in the array of microcavities. The size of the vortex core as well as the phase gradients, corresponding to the radial superflows, and the shape of the vortex trajectories are not significantly influenced by moderate variations of  $\kappa$ .

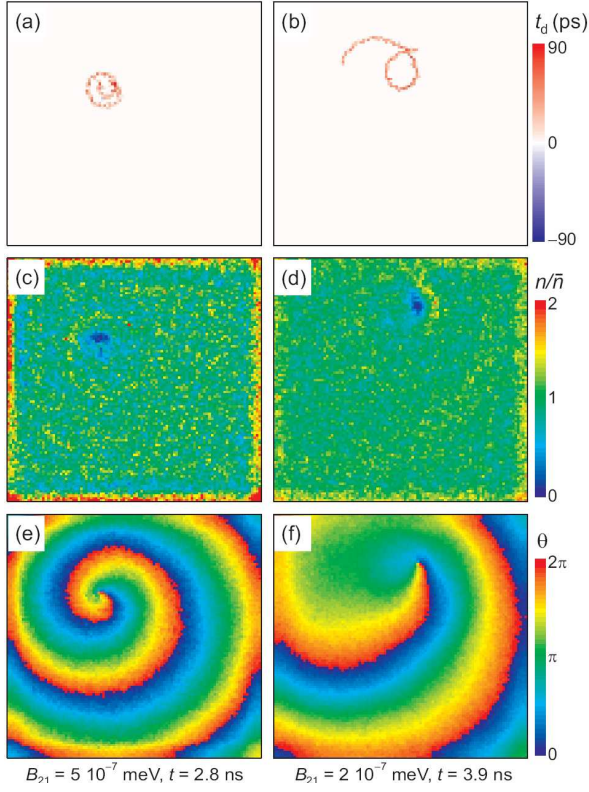


FIG. s3. Vortex trajectories within the time interval  $(0, t)$  [panels (a) and (b)] and snapshots of the photon density  $n$  [panels (c) and (d)] and the phase of the order parameter  $\theta$  [panels (e) and (f)] at the time moment  $t$  for  $\Delta/(k_B T) = -7.2$ ,  $M = 5 \times 10^{10}$ ,  $\bar{n} = 5 \times 10^4$ ,  $J = 0.02$  meV,  $\gamma = 0.005$  meV,  $\kappa = 0.153$  meV ( $\kappa$  is considered here as an independent parameter) and two different values of  $B_{21}$ :  $B_{21} = 5 \times 10^{-7}$  meV [panels (a), (c) and (e)] and  $B_{21} = 2 \times 10^{-7}$  meV [panels (b), (d) and (f)]. When decreasing  $B_{21}$ , the exchange between the photon subsystem inside each microcavity and the molecule reservoir slows down as compared to the intercavity exchange due to the Josephson coupling. This is accompanied by a reduction of phase gradients in the radial direction and a decrease of the curvature of the vortex trajectory. At the same time, a decrease of  $B_{21}$  leads to the corresponding weakening of the phase and density fluctuations, caused by the spontaneous emission of photons in each microcavity.



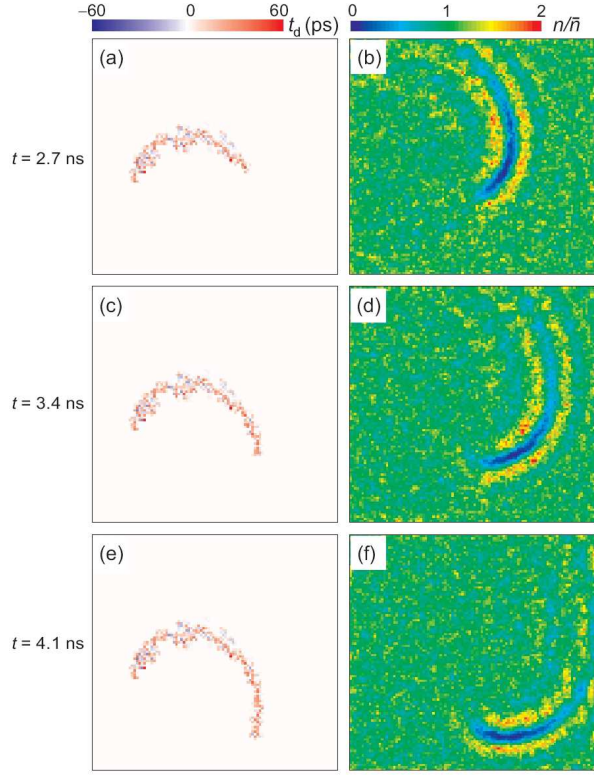


FIG. s4. Vortex trajectories within the time interval  $(0, t)$  [panels (a), (c) and (e)] and snapshots of the photon density  $n$  [panels (b), (d) and (f)] at the time moment  $t$  for  $k_B T = 25$  meV,  $\Delta/(k_B T) = -7.2$ ,  $M = 5 \times 10^{10}$ ,  $\bar{n} = 5 \times 10^4$ ,  $J = 0.02$  meV,  $\gamma = 0.02$  meV,  $B_{21} = 2.5 \times 10^{-8}$  meV and different  $t$ :  $t = 2.7$  ns [panels (a) and (b)],  $t = 3.4$  ns [panels (c) and (d)], and  $t = 4.1$  ns [panels (e) and (f)]. The reorientation of the elongated vortex core with time is seen to be retarded with respect to the changes of the vortex motion direction.

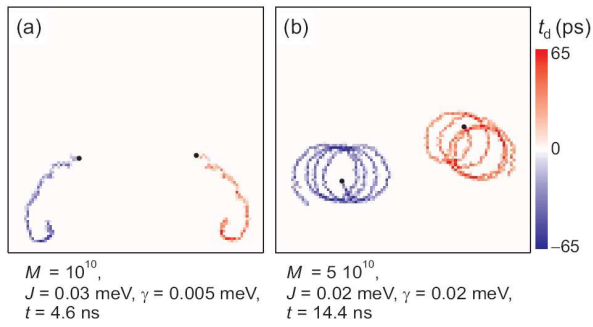


FIG. s5. Vortex (red) and antivortex (blue) trajectories within the time interval  $(0, t)$  for  $M = 10^{10}$ ,  $J = 0.03$  meV,  $\gamma = 0.05$  meV,  $t = 4.6$  ns (a) and  $M = 5 \times 10^{10}$ ,  $J = 0.02$  meV,  $\gamma = 0.02$  meV,  $t = 14.4$  ns (b). Other parameters are  $k_B T = 25$  meV,  $\Delta/(k_B T) = -7.2$ ,  $\bar{n} = 5 \times 10^4$ ,  $B_{21} = 10^{-7}$  meV. The black circles indicate the (anti)vortex positions at  $t = 0$ . The overall direction of vortex motion corresponds to the presence of a (long-range) vortex-antivortex repulsion.